



Two Pyrophosphates with Large Birefringences and Second-Harmonic Responses as Ultraviolet Nonlinear Optical Materials

Xuefang Lu, Zhaohui Chen,* Xuerui Shi, Qun Jing,* and Ming-Hsien Lee

Abstract: Two new pyrophosphates nonlinear optical (NLO) materials, $Rb_3PbBi(P_2O_7)_2$ (**I**) and $Cs_3PbBi(P_2O_7)_2$ (**II**), were successfully designed and synthesized. Both compounds exhibit large NLO effects and birefringences. Material **I** presents the scarce case of possessing the coexistence of large birefringence (0.031 at 1064 nm and 0.037 at 532 nm) and second harmonic generation (SHG) response ($2.8 \times$ potassium dihydrogen phosphate (KDP)) in ultraviolet NLO phosphates and its SHG is the largest in the phase-matching (PM) pyrophosphates. Both **I** and **II** have three-dimensional (3D) crystal structures composed of corner-shared RbO_{12} (CsO_{11}), RbO_{10} (CsO_{10}), BiO_6 , PbO_7 (PbO_6) and P_2O_7 groups, in which P_2O_7 and PbO_7 (PbO_6) units form an alveolate $[PbPO]_{\infty}$ skeleton frame. Theoretical calculations reveal that the P–O, Bi–O and Pb–O units are mainly responsible for the moderate birefringence and large SHG efficiency of **I**.

Introduction

Compared with electrons, photons have many advantages in transmitting information. Photons nonlinear optics (NLO) is an emerging field of photonics, in which photons instead of electrons and are used for signal transmission and processing.^[1] This is especially true for high performances ultraviolet (UV) NLO materials, which are the hard-core parts of solid-state laser.^[2] They can generate coherent and tunable laser beams by cascaded second harmonic or difference frequency generation (SHG and DFG), which cover UV, visible, infrared (IR), and even terahertz spectra regions. For NLO materials, moderate birefringence and large SHG coefficient are imminent demands, which can guarantee the phase-matching (PM) in desired wavelength range and high laser conversion efficiency.^[3] Consequently, it is still great academic demand to obtain the NLO materials possessing both traits from the perspective of structural design.

Borates are inspiring systems for seeking UV NLO and birefringence materials due to their outstanding hyperpolarizabilities and anisotropies.^[4] Based on mature NLO materials

(β - BaB_2O_4),^[5] LiB_3O_5 ,^[6] and $KBe_2BO_3F_2$ ^[7]) and unique birefringent crystals (α - BaB_2O_4)^[8] and $Ca(BO_2)_2$ ^[9]), a series of excellent UV or deep-UV NLO borates with active-NLO chromophores or halide ions have been developed.^[10] Most recently, new $[BO_xF_{4-x}]^{(x+1)-}$ ($x=1, 2, 3$) tetrahedra with multifaceted good characteristics as building blocks were introduced, which led to a series of high performances NLO crystals.^[11]

Phosphate structures are commonly rigid, which beneficial to enhance the chemical and thermally stabilities. Especially, $[PO_4]^{3-}$ is resistant absorb in UV/Vis region and so solid phosphates are also ideal candidates as UV NLO materials, which show a huge variety of crystal configurations and are relatively unexplored. We reviewed about recent phosphates, such as $Ba_3P_3O_{10}Cl$ (180 nm, $0.6 \times$ KDP, 0.023 @ 1064 nm),^[12] $K_4Mg_4(P_2O_7)_3$ (170 nm, $1.3 \times$ KDP, 0.0108 @ 1064 nm),^[13] $Ba_5P_6O_{20}$ (167 nm, $0.8 \times$ KDP),^[14] $KLa(PO_3)_4$ (162 nm, $0.7 \times$ KDP, 0.0084 @ 1064 nm),^[15] $CsLa(PO_3)_4$ (167 nm, $0.5 \times$ KDP, 0.0068 @ 1064 nm),^[16] $Ba_2NaClP_2O_7$ (< 176 nm, $0.9 \times$ KDP, 0.017 @ 1064 nm).^[17] For most of them, they either exhibit weak SHG responses or small birefringence in spite of their short cut-off UV edges, which hinder their conversion efficiency and PM abilities. To achieve the enhanced second-order susceptibility and birefringence, introducing NLO-active groups into non-centrosymmetric (NCS) solid phosphates is an effective approach. These NLO-active groups possess polyhedra with distorted electronic orbits, such as stereochemically active d^0 or ns^2 lone pair cations,^[18] however accompanied with undesired red-shifting possibility. To achieve the balance of the tripartite confrontation, that is, SHG efficiency, birefringence and UV cutoff edge, introducing ns^2 lone pair cations is a favorable and effective strategy. It is attributed to two reasons: (1) the activity of stereochemically active lone pair may be maintained to an ideal degree. (2) the ns^2 lone pair cations have the less negative effect relative to other NLO-active cations in terms of redshift of cut-off edge. Considering the cooperative effect of the multiple NLO-active constructing groups, we put forth effort to combine two different ns^2 lone pair cations Bi^{3+} , Pb^{2+} with P–O group, as well as Cs^+ or Rb^+ cation without UV absorption and successfully synthesized two pyrophosphates $Rb_3PbBi(P_2O_7)_2$ (**I**) and $Cs_3PbBi(P_2O_7)_2$ (**II**). **II** was first prepared by Igor V. Zatovsky et al. in 2018 but without the report on its NLO performances.^[19] Compounds **I** and **II** have the remarkable SHG effects and birefringences, that is 2.8 , $1.1 \times$ KDP and 0.031 , $0.020@1064$ nm, while with short UV cutoff edges 285 and 275 nm, respectively. Fortunately, an effective balance has been achieved involving the above important factors for both compounds. It is noteworthy that compound **I** has the strongest SHG effect among the

[*] X. F. Lu, Prof. Z. H. Chen, X. R. Shi, Prof. Q. Jing
College of Chemistry and Chemical Engineering & School of Physical Science and Technology, Xinjiang University
666 Shengli Road, Urumqi 830046 (China)
E-mail: chenzhaohui@xju.edu.cn
qunjing@xju.edu.cn

Prof. M. H. Lee
Department of Physics, Tamkang University
New Taipei City 25137 (Taiwan)

Supporting information and the ORCID identification number(s) for the author(s) of this article can be found under:
<https://doi.org/10.1002/anie.202007494>

known pyrophosphates NLO materials and breaks through the $2 \times$ KDP boundary accompanied with large birefringence and short cut-off edge simultaneously. In addition, the synthesis, thermal behavior, and optical properties of compounds **I** and **II** were presented. The experimental and theoretical calculation results show that both of them are excellent candidates for UV NLO utilities.

Results and Discussion

Crystal Structure Description. **I** crystallizes in monoclinic chiral and polar space group $P2_1$ (No. 4) presenting a unique structure type. Differing from **I**, **II** crystallizes into the biaxial orthorhombic crystal system with chiral and non-polar space group $P2_12_12_1$ (No. 19). The complete structure of **I** exhibits a three-dimensional (3D) network, which composed of RbO_{12} , RbO_{10} , BiO_6 , PbO_7 and P_2O_7 groups. In the structure, isolated P (3,4) $_2\text{O}_7$ and PbO_7 polyhedra connect with each other via sharing edge and vertex oxygen atoms to extend a two-dimensional (2D) alveolate $[\text{PbP}_2\text{O}_9]_\infty$ layers parallel to the c -axis (Figure 1b). The $[\text{PbP}_2\text{O}_9]_\infty$ layers are stacked along the a axis and connect with each other by oxygen atoms of $\text{P}(1,2)_2\text{O}_7$ group to form a 3D framework with interstitial voids, in which Rb^+ and Bi^{3+} cations reside along the $[100]$ plane (Figure 1a). In light of the topology, two PbO_7 polyhedra and four $[\text{PO}_4]^{3-}$ tetrahedra act as nodes to form a honeycomb-like pentagonal net in $[\text{PbP}_2\text{O}_9]_\infty$ single layer (Figure 1c). The structure may be described as $\{[\text{PbO}_{7/2}]^{5-} [\text{P}(1,2)_2\text{O}_{5/1}\text{O}_{2/2}]^{2-} [\text{P}(3,4)_2\text{O}_{2/1}\text{O}_{5/2}]^{1+}\}^{6-}$ in connectivity terms, with the charge balanced by Rb^+ and Bi^{3+} cations.

The crystal **II** exhibits a similar framework to **I**, which composed of CsO_{11} , CsO_{10} , PbO_6 , BiO_6 , P_2O_7 polyhedra. The crystal structure of compound **II** is schematically shown in Figure 2, PbO_6 and $\text{P}(3,4)_2\text{O}_7$ alternately connect with each other via sharing vertex oxygen atoms to build $[\text{PbP}_2\text{O}_{10}]_\infty$ double chains along the b axis. Apparently, seen along the $[001]$ direction, those adjacent double chains linked together by the $\text{P}(1,2)_2\text{O}_7$ groups forming a $[\text{PbP}_4\text{O}_{12}]_\infty$ layer, and then layers successively stretch along the a axis to constitute a 3D network structure. The structure may be described as follows $\{[\text{PbO}_{6/2}]^{4-} [\text{P}(1,2)_2\text{O}_{4/1}\text{O}_{3/2}]^{1-} [\text{P}(3,4)_2\text{O}_{4/1}\text{O}_{3/2}]^{1-}\}^{6-}$ in connectivity terms, with the charge balanced by the Cs^+ and Bi^{3+} cations.

I and **II** are not iso-structural despite exhibiting the same chemical formulas and similar 3D frameworks. Although both

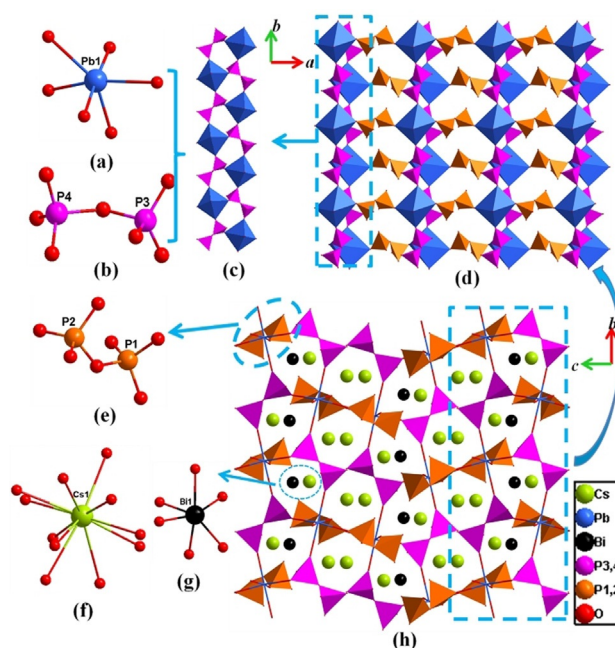


Figure 2. The crystal structure of **II**. a) PbO_6 unit; b) $\text{P}(3,4)_2\text{O}_7$ unit; c) The double chain $[\text{PbP}_2\text{O}_{10}]_\infty$; d) $[\text{PbP}_4\text{O}_{12}]_\infty$ layer along the c axis; e) $\text{P}(1,2)_2\text{O}_7$ unit; f) $\text{Cs}(1)\text{O}_{11}$ polyhedron; g) BiO_6 polyhedron; h) 3D framework along the a axis.

compounds exhibit $[\text{PbPO}]_\infty$ single-layers, the orientation of them are different, attributing to the different space group, $P2_1$ and $P2_12_12_1$. Two inverse orientations of the $[\text{PbP}_4\text{O}_{12}]_\infty$ layer, labeled A and A', are observed in **II**, which has three 2_1 -screw axes (Figure 3b). Whereas, in **I**, $[\text{PbP}_2\text{O}_9]_\infty$ layers arrange parallel along the c axis (Figure 3a). More notably, the connection mode of Pb^{2+} and Bi^{3+} cations with lone-pair electrons is shown Figure 4. In compound **I**, PbO_7 and BiO_6 polyhedra interconnect via a vertex O to form a zigzag 1D $[\text{PbBiO}_{12}]_\infty$ chain along the b axis. The 1D $[\text{PbBiO}_{12}]_\infty$ chains are paralleled to each other in the ab -plane, whereas in **II**, PbO_6 and BiO_6 polyhedra construct to zero-dimensional (0D) $[\text{PbBiO}_{11}]^{17-}$ dimers with back-to-back pattern. The packings of crystals **I** and **II** should have relation with the different atomic sizes of Rb and Cs atoms. The Pb-O polyhedra, i.e., the seven-fold coordinated PbO_7 polyhedra, have Pb-O bonds lengths ranging from 2.27(2) Å to 2.761(11) Å in **I** vs. the six-fold coordinated PbO_6 polyhedra with Pb-O bonds in the range of 2.456(6) Å–2.752 (6) Å in **II**. From above

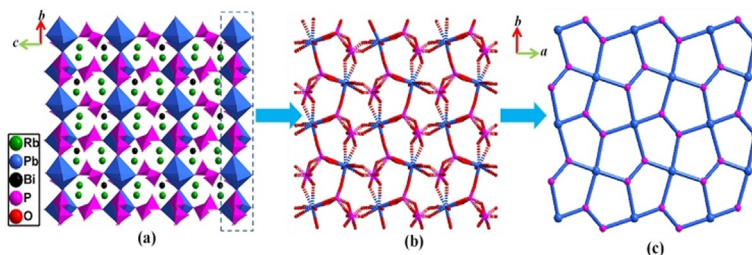


Figure 1. a) Crystal structure of **I**, in which $[\text{PbP}_2\text{O}_9]_\infty$ layers stack along the a axis; b) $[\text{PbP}_2\text{O}_9]_\infty$ layer composed of $\text{P}(3,4)_2\text{O}_7$ dimers, viewed along the c axis; c) Topological structure of a $[\text{PbP}_2\text{O}_9]_\infty$ single layer. The blue spheres and pink spheres represent PbO_7 , PO_4 polyhedra, respectively.

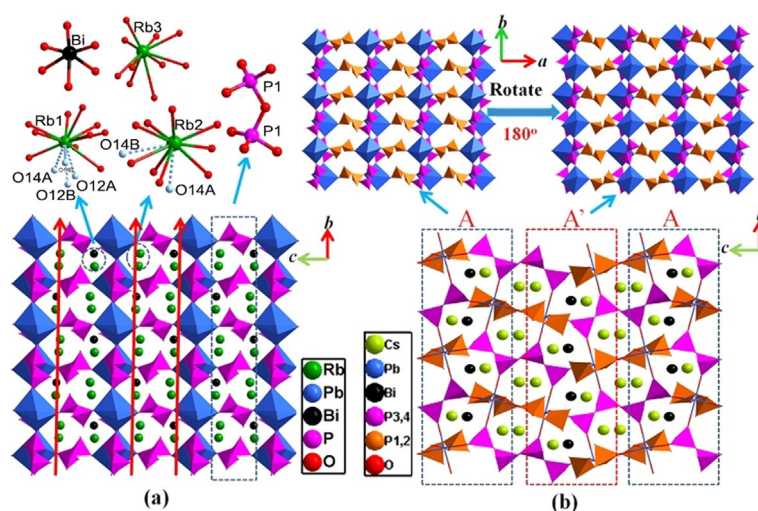


Figure 3. A structural comparison of a) **I** and b) **II**. **I** contains a single orientation of the $[\text{PbP}_4\text{O}_{12}]_\infty$ single-layer with the stretched $\text{P}(1,2)_2\text{O}_7$ group connecting the 3D framework, whereas **II** contains two inverse orientations of the $[\text{PbP}_4\text{O}_{12}]_\infty$ single-layer.

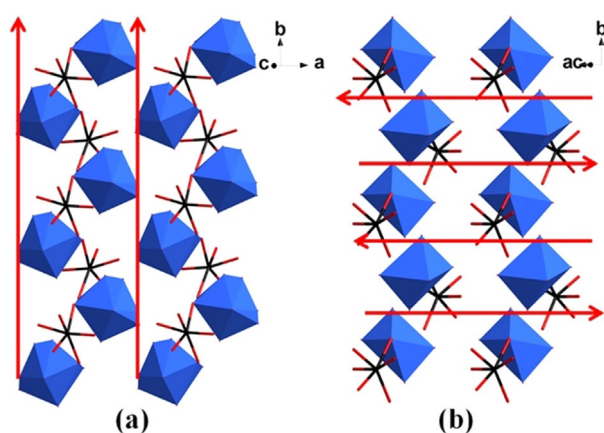


Figure 4. a) a zigzag 1D $[\text{PbBiO}_{12}]_\infty$ chain along the b axis for **I**; b) zero-dimensional (0D) $[\text{PbBiO}_{11}]^{17-}$ dimers for **II**.

presentation, we deduce that the synergistic effects of favorable honeycomb-like $[\text{PbP}_2\text{O}_9]_\infty$ layers and 1D paralleled $[\text{PbBiO}_{12}]_\infty$ chains for **I** are the main contributor for the SHG and birefringence. Additionally, each P atom is bonded to four oxygen atoms with P–O bond lengths vary between 1.38(2) and 1.70(2) Å, and Bi atoms are bonded to six atoms with Bi–O bond lengths ranging from 2.181(11) to 2.618(6) Å. The Rb atoms are 10-coordinated to form three types RbO_8 polyhedra with Rb–O distances ranging from 2.76(2) to 3.576 (12) Å, while the Cs atoms exhibit 10- and 11-coordinate environments with Cs–O distances ranging from 3.033(7) to 3.790(7) Å. All bond lengths are in reasonable ranges.

IR Spectra. To verify the presence of structure units, the IR spectra of the title compounds were measured at room temperature in the 400–4000 cm^{-1} range (Supporting Information, Figure S2). **I** and **II** have the similar spectra and the sharp peaks between 888 and 863 cm^{-1} are likely assigned as the asymmetric stretching vibration for P–O–P bridge, whereas several peaks in the range from 696 to 719 cm^{-1} are attributed to the symmetric P–O–P stretching vibration. In

addition, the intense absorption bands around 1128–987 cm^{-1} play important roles to the asymmetric and symmetric stretching vibration of O–P–O bonds, while the strong peaks at 525–565 cm^{-1} are due to the fundamental frequency of the PO_4 building. These assignments match well with the reported results.

Thermal Behaviors. Thermogravimetric and Differential Thermal Analysis (TG-DTA) measurements were carried out for investigating the thermal properties of **I** and **II** and the consequences are shown in Figure S3. Results of TG suggest that there is nearly no weight loss before 1000 °C for them. In addition, for **I** and **II** only exhibit endothermic peaks around 564 °C and 660 °C on the heating curves, respectively. The remnants were transparent glass after TG and DTA test because of high viscosity, which also was verified by the smooth cool curves of them. To further investigate the thermal behaviors, the powders of **I** and **II** were melted at 800 °C for 24 h and slowly cooled to ambient temperature at a rate of 2 °C h⁻¹. The powder XRD patterns of the before- and after-melting polycrystalline samples demonstrate that **II** is congruent melting compound, while **I** is incongruent and suitable for growing large sized crystals by flux method (Figure 5).

UV/Vis-IR Diffuse Reflectance Spectrum. Commonly, the smaller cationic radius is helpful to obtain larger band-gap energies for the similar chemical formula. As shown in Figure 6, the UV/Vis-IR spectra display that the experimental band gaps of the title compounds are 4.35 eV and 4.68 eV, respectively, which are larger than the most Bi (Pb)-based phosphates, for example, $\text{Rb}_2\text{PbBi}_2(\text{PO}_4)_2(\text{P}_2\text{O}_7)$ (4.29 eV),^[20] $\text{Cs}_2\text{PbBi}_2(\text{PO}_4)_2(\text{P}_2\text{O}_7)$ (4.25),^[20] $\text{Pb}_3\text{Bi}(\text{PO}_4)_3$ (3.97 eV),^[21] $\text{Cd}_3\text{Bi}(\text{PO}_4)_3$ (3.90 eV),^[21] $\text{Sr}_3\text{Bi}(\text{PO}_4)_3$ (4.09 eV)^[21] and $\text{Ca}_3\text{Bi}(\text{PO}_4)_3$ (4.20 eV).^[21] We inferred that the Pb^{2+} cations with larger ion radius and lone pair electrons may have less effect on narrowing the band-gap between the conduction and valence bands of **I** and **II**.

SHG Measurements and the Origin of the Enhancement. SHG measurements were performed on both compounds

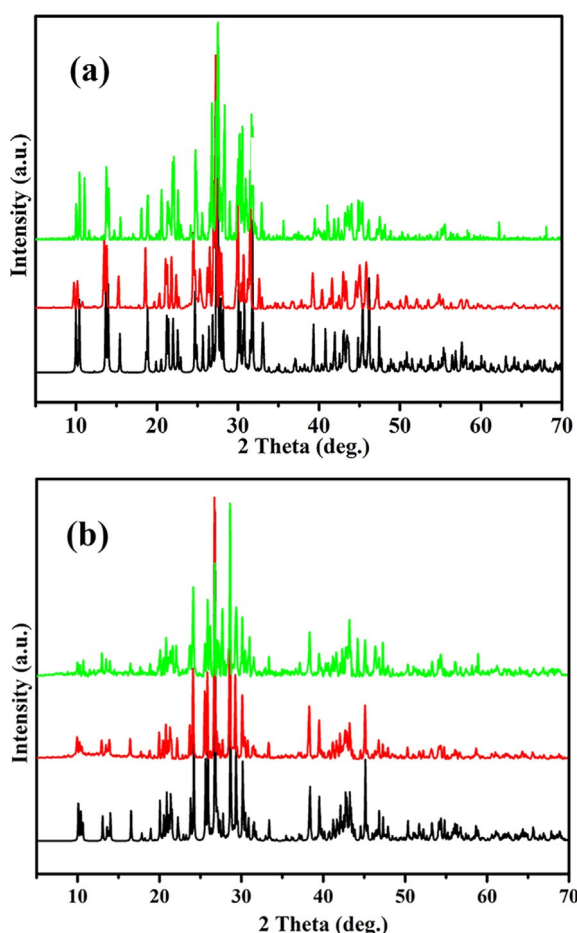


Figure 5. PXRD patterns of the title compounds before and after melting a) **I** and b) **II**. Key: after melting (green), before melting (red), calculated (black).

since they crystallize in the NCS space groups. Using 1064 nm radiation, the result revealed their SHG responses are ≈ 2.8 and 1.1 times that of KDP for the compound **I** and **II** in the 200–225 μm particle size range, respectively. As shown in Figure 7, we also carried out SHG measurements in the range of 20–225 μm . The SHG intensities increase with increasing particle sizes until particle sizes are independent and so both compounds are type **I** PM according to the rule proposed by Kurtz and Perry.^[22] Noteworthy, **I** is the largest known to date in PM UV NLO pyrophosphates, such as $\text{CsLiCdP}_2\text{O}_7$ ($1.5 \times \text{KDP}$),^[23] $\text{K}_4\text{Mg}_4(\text{P}_2\text{O}_7)_3$ ($1.3 \times \text{KDP}$),^[13] $\text{Rb}_4\text{Mg}_4(\text{P}_2\text{O}_7)_3$ ($1.4 \times \text{KDP}$),^[13] $\text{Ba}_2\text{NaClP}_2\text{O}_7$ ($0.9 \times \text{KDP}$),^[17] as well as $\text{CsNaMgP}_2\text{O}_7$ ($1.1 \times \text{KDP}$)^[24] and $\text{RbNaMgP}_2\text{O}_7$ (HTP) ($1.4 \times \text{KDP}$)^[25] (Table 1).

It is well known that the SHG effects of low polymerized pyrophosphates with short absorption edges are usually smaller.^[32] Normally, the origins of NLO efficiency are critically dependent on the asymmetry and alignment of polyhedra in the crystal structure. Pb^{2+} and Bi^{3+} cations belong to the sixth-period, which have less stereoactive nature relative to the fourth or fifth period cations.^[36] In compound **I**, PbO_7 and BiO_6 polyhedra interconnect to form zigzag 1D $[\text{PbBiO}_{12}]_{\infty}$ chains and are paralleled to each other in the *ab*-plane, whereas in compound **II**, Pb^{2+} and Bi^{3+} cations both

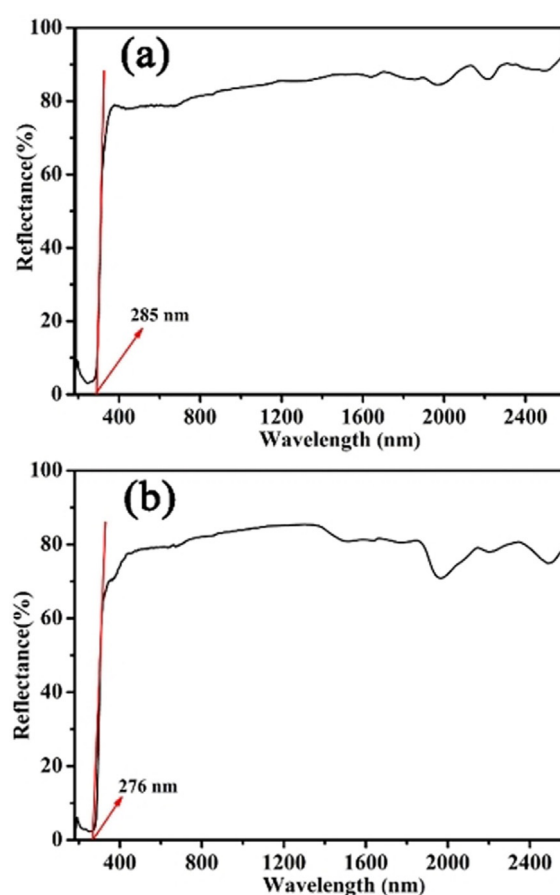


Figure 6. The UV/Vis-NIR diffuse reflectance spectra of a) **I** and b) **II**.

form irregular PbO_6 and BiO_6 octahedra with increasing lone pair electron stereochemical activity, but constructing 0D $[\text{PbBiO}_{11}]^{17-}$ dimers and aligning in the opposite direction. The unfavorable configuration of these microscopic $[\text{PbBiO}_{11}]^{17-}$ dimers lead to the decreased overall second-order susceptibility for compound **II**. We can expect that if these active microscopic $[\text{PbBiO}_{11}]^{17-}$ dimers align in good manners, the SHG of crystal **II** should be apparently enhanced. These structural analyses give us some enlightenment to design NLO materials with enhanced SHG effects.

Electronic Structures and Optical Properties. Using the method described in SI, the band structures of crystals **I** (both RbPbBi531 and RbPbBi469) and **II** are obtained. Noting that, the obtained band gaps of RbPbBi531 , and RbPbBi469 are both 4.23 eV (shown in Figure 8a, and Figure S4a in the SI, respectively). The obtained refractive indices, birefringences of RbPbBi531 and RbPbBi469 (as shown in Figure 9a and Figure S5, respectively) and SHG response are all similar, hence take the RbPbBi531 model as an example to discuss the electronic structures and optical properties of compound **I**.

The obtained band structures are presented in Figure 8a and Figure 10a. The compounds **I** and **II** possess band gaps of 4.23 and 4.18 eV, respectively, which are slightly smaller than those of the experimental values. The underestimation of band gaps has relation with the derivative discontinuity of the exchange correlation energy.^[37]

Table 1: Space groups, SHG responses, calculated SHG coefficients, birefringences and phase-matchable for the UV phosphate NLO materials.

SHG active phosphates	Comp.	S.G.	PSHG (×KDP)	d_{ij} (pm/V)	Cal. birefringence	PM	
orthophosphates	LiRb ₂ PO ₄ ^[26]	<i>Cmc2</i> ₁	2.1	$d_{31}=0.46$; $d_{24}=0.11$; $d_{33}=0.28$	–	PM	
	LiCs ₂ PO ₄ ^[27]	<i>Cmc2</i> ₁	2.6	$d_{31}=-0.65$; $d_{24}=0.22$; $d_{33}=0.61$	–	PM	
	LiPbPO ₄ ^[28]	<i>Pna2</i> ₁	3	$d_{15}=-1.05$; $d_{24}=-0.24$; $d_{33}=4.52$	–	NPM ^[a]	
	Sr ₃ Zn ₃ TeP ₂ O ₁₄ ^[29]	<i>P321</i>	2.8	$d_{11}=2.27$	–	PM	
	Ba ₃ Zn ₃ TeP ₂ O ₁₄ ^[29]	<i>P321</i>	3	$d_{11}=2.33$	–	PM	
	Pb ₃ Zn ₃ WP ₂ O ₁₄ ^[29]	<i>P321</i>	7	$d_{11}=3.91$	–	PM	
	Pb ₃ Mg ₃ TeP ₂ O ₁₄ ^[30]	<i>P321</i>	13.5	$d_{11}=4.96$	–	PM	
	Pb ₃ Zn ₃ TeP ₂ O ₁₄ ^[29]	<i>P321</i>	13.5	$d_{11}=4.96$	–	PM	
	pyrophosphates	Ba ₂ NaClP ₂ O ₇ ^[17]	<i>P4bm</i>	0.9	$d_{ave}=1.11$	0.017@1064 nm	PM
		CsNaMgP ₂ O ₇ ^[24]	<i>Cmc2</i> ₁	1.1	$d_{31}=0.368$; $d_{32}=-0.178$; $d_{33}=-0.321$	–	PM
RbNaMgP ₂ O ₇ ^[25] (LTP)		<i>Pna2</i> ₁	0.9	N/A	0.031@532 nm	PM	
RbNaMgP ₂ O ₇ ^[25] (HTP)		<i>Ccm2</i> ₁	1.4	N/A	0.035@532 nm	PM	
CsLiCdP ₂ O ₇ ^[23]		<i>Pmc2</i> ₁	1.5	N/A	–	PM	
LiNa ₃ P ₂ O ₇ ^[31]		<i>C222</i> ₁	0.25	N/A	–	–	
LiK ₃ P ₂ O ₇ ^[31]		<i>C222</i> ₁	0.2	N/A	–	–	
Rb ₂ Ba ₃ (P ₂ O ₇) ₂ ^[32]		<i>P2₁2₁2₁</i>	0.3	$d_{14}=0.073$	–	NPM ^[a]	
Cs ₂ Ba ₃ (P ₂ O ₇) ₂ ^[33]		<i>P2₁2₁2₁</i>	0.4	$d_{14}=0.15$	–	–	
K ₄ Mg ₄ (P ₂ O ₇) ₃ ^[13]		<i>Pc</i>	1.3	–	0.007@1064 nm	PM	
Rb ₄ Mg ₄ (P ₂ O ₇) ₃ ^[13]		<i>Amm2</i>	1.4	–	0.0108@1064 nm	PM	
Rb₃PbBi(P₂O₇)₂		<i>P2₁</i>	2.8	$d_{14}=-0.085$; $d_{16}=1.21$; $d_{22}=0.29$; $d_{23}=-0.40$	0.031@1064 nm	PM	
Cs₃PbBi(P₂O₇)₂		<i>P2₁2₁2₁</i>	1.1	$d_{14}=0.30$	0.037@532 nm	PM	
triphosphates		Ba ₃ P ₃ O ₁₀ Br ^[12]	<i>P2₁2₁2₁</i>	0.5	$d_{ave}=0.49$	0.023@1064 nm 0.024@532	PM
		Ba ₃ P ₃ O ₁₀ Cl ^[12]	<i>Pca2</i> ₁	0.6	$d_{ave}=0.57$	0.028@1064 nm 0.030@532 nm	PM
		Ba ₅ P ₆ O ₂₀ ^[14]	<i>Pca2</i> ₁	0.8	N/A	–	PM
polyphosphates		RbBa ₂ (PO ₃) ₅ ^[32]	<i>Pc</i>	1.4	$d_{11}=-0.066$; $d_{12}=0.371$; $d_{13}=-0.591$; $d_{15}=0.007$; $d_{24}=0.197$; $d_{33}=0.073$	–	PM
	KBa ₂ (PO ₃) ₅ ^[34]	<i>Pc</i>	0.9	0.265–0.276	–	PM	
	KLa(PO ₃) ₄ ^[15]	<i>P2₁</i>	0.7	$d_{14}=-0.574$; $d_{16}=0.56$; $d_{22}=-0.585$; $d_{23}=0.585$	0.0084@1064 nm	PM	
	CsLa(PO ₃) ₄ ^[16]	<i>P2₁</i>	0.5	–	0.0068@1064	NPM ^[a]	
	KPb ₂ (PO ₃) ₅ ^[35]	<i>Pn</i>	0.5	–	–	PM	
	RbPb ₂ (PO ₃) ₅ ^[35]	<i>Pn</i>	0.3	–	–	PM	

[a] Non-phase matching (NPM).

The projected density of states (PDOS) of compounds **I** and **II** are also obtained. As shown in Figure 8b and Figure 10b, the two compounds own similar feature of PDOS and so we took **I** as an example. At the top of the valence band (from –10 eV to the Fermi level), there are O-sp, P-sp, Bi-sp, Pb-sp and isolated Rb-p states and at the bottom of the conduction band, the states mainly come from O, P, Bi, and Pb atoms. The hybrid P-O, Pb-O, and Bi-O chemical bonds are found at the top of the valence band near the Fermi level, which would give main contribution to the optical properties of the compound **I**. Using the method described in SI, the refractive indices and birefringences of crystal **I** and **II** are also obtained. As shown in Figure 9, the crystal **I** owns relative large birefringence as 0.031@1064 nm and 0.037@532 nm, while the crystal **II** owns birefringence as 0.020@1064 nm and 0.023@532 nm. As we know that due to

the rigid structure of PO₄ tetrahedron, many phosphates own relative small birefringences, such as Ba₂NaClP₂O₇ (0.017 at 1064 nm),^[17] KLa(PO₄)₃ (0.008 at 1064 nm),^[15] CsLa(PO₄)₃ (0.0068 at 1064 nm)^[16] and so on (shown in Table 1). The birefringence of the **I** is comparable to RbNaMgP₂O₇ (0.035 (HTP) and 0.031 (LTP) at 532 nm, respectively),^[25] Ba₃P₃O₁₀Br (0.023 at 1064 nm and 0.024 at 532 nm)^[12] and Ba₃P₃O₁₀Cl (0.028 at 1064 nm and 0.030 at 532 nm).^[12]

As described above, from the states among the Fermi level, we can deduce that the P-O, Pb-O, and Bi-O polyhedra would give main contribution to the optical properties of **I** (RbPbBi531). To better understand the contribution from these polyhedra to the birefringence, we employed real-space atom-cutting method.^[38] The Mulliken bond population showed that the P–O bonds own the bond population as 0.78 –0.38, indicating have more covalent bond features for

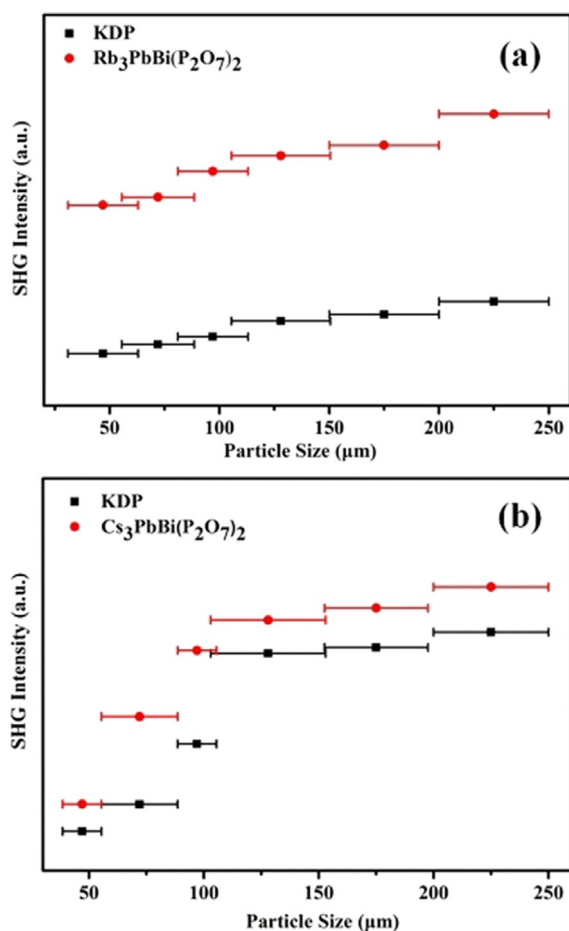


Figure 7. The powder SHG measurements at 1064 nm of a) I and b) II.

P–O bonds while the Bi–O and Pb–O bonds own the Mulliken bond population as 0.26–0.18 and 0.15–0.13, respectively, implying have more ionic bond characters, especially for Pb–O bonds. Hence, the atom-cutting radii are set as 1.48, 1.20, 1.20 Å for Rb, Pb and Bi, meanwhile 1.06 and 0.90 Å for P and O, respectively. The one named keep-BiO (keep-PbO, and keep-PO) means the optical properties obtained by BiO (PbO or PO) groups while other ionic groups were removed. As shown in Table 2 and Figure 11, the birefringences of BiO, PbO and PO own the sequence as keep-BiO > keep-PO > keep-PbO, implying the P–O and Bi–O groups give main contribution to the total birefringence.

The SHG tensors of crystal I and II are also calculated. For crystal I which crystallized in $P2_1$ space group, there are four different nonzero SHG tensors: $d_{16} = 1.21 \text{ pm V}^{-1}$, $d_{14} = -0.085 \text{ pm V}^{-1}$, $d_{22} = 0.49 \text{ pm V}^{-1}$, $d_{23} = -0.40 \text{ pm V}^{-1}$, respectively. The maximum value d_{16} is about $3.10 \times \text{KDP}$, which is comparable with the experimental value (about $2.8 \times \text{KDP}$). The calculated effective SHG response is about 0.87 pm V^{-1} , which is about $2.65 \times \text{KDP}$.^[22,39] For crystal II, the obtained SHG tensor is $d_{14} = 0.30 \text{ pm V}^{-1}$, and the evaluated effective SHG response is about $0.77 \times \text{KDP}$, which are slightly smaller than that of the experimental value (about $1.1 \times \text{KDP}$). Using the real-space atom-cutting method, the SHG responses from different groups of crystal I are also obtained. As shown in Table 3, taking the largest SHG tensor d_{16} as example, the

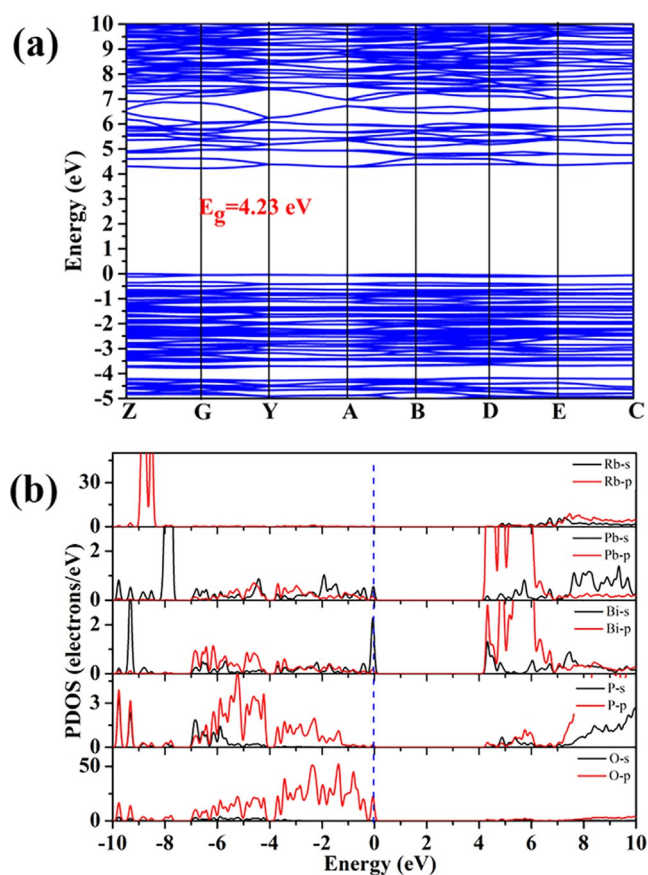


Figure 8. Electronic properties of I. a) Band structure. b) Projected density of states (PDOS).

Table 2: The obtained birefringence (@1064 nm) of I (RbPbBi531) model after the PO, PbO, and BiO polyhedra were removed using the real-space atom-cutting method.

Crystal	Contributions	n_x	n_y	n_z	Δn
I (RbPbBi531)	Keep-PbO	1.398	1.397	1.387	0.011
	Keep-PO	1.596	1.583	1.575	0.021
	Keep-BiO	1.428	1.408	1.401	0.027
	Origin	1.772	1.752	1.741	0.031

BiO, PO, and PbO ionic groups give contribution about 51 %, 59 %, and 67 %, respectively. The sum of SHG response from BiO, PO, and PbO is larger than the total SHG response of crystal I, which may have relation with the bridge oxygen atoms between these polyhedra.

Conclusion

Two promising UV NLO materials, $\text{Rb}_3\text{PbBi}(\text{P}_2\text{O}_7)_2$ (I) and $\text{Cs}_3\text{PbBi}(\text{P}_2\text{O}_7)_2$ (II), have been obtained. We introduced $[\text{PbPO}]_\infty$ layers and BiO_6 polyhedra containing two types of lone-pair cations into both compounds. Notably compound I achieves multiple criteria balances, that is, moderate birefringence, large microscopic SHG coefficients while it retains a UV transparency window. These qualities manifest that I

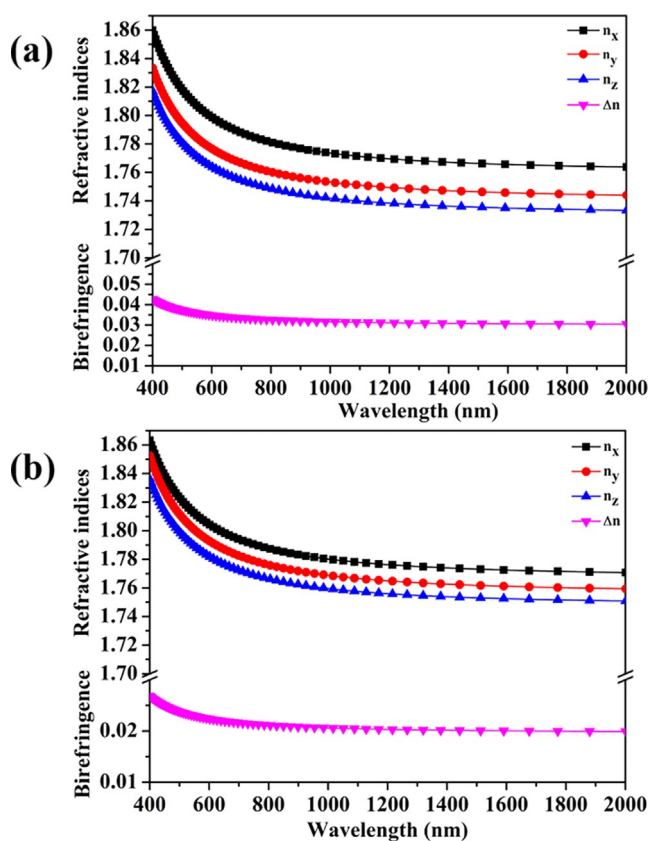


Figure 9. The obtained refractive indices and birefringences of a) I (RbPbBi531) and b) II.

Table 3: The obtained SHG response of I (RbPbBi531) from different ionic groups obtained by real-space atom-cutting method.

Crystal	Contributors	112	123	222	233
I (RbPbBi531)	Keep-BiO	0.616	0.317	0.349	0.049
	Keep-PO	0.715	-0.414	0.390	-0.294
	Keep-PbO	0.816	-0.110	0.668	-0.265
	Origin	1.207	-0.086	0.490	-0.398

panders to the considerable factors as a promising UV NLO material. The structure analysis reveals that the observed optical properties of compound I is mainly ascribed to the honeycomb-like $[\text{PbP}_2\text{O}_9]_\infty$ single layer and the parallel $[\text{PbBiO}_{12}]_\infty$ chain combining stereoactive lone-pairs of Pb^{2+} and Bi^{3+} . This study provides a feasible way to design pyrophosphates with large SHG ($> 2 \times \text{KDP}$) and we are in the process of designing new polar NLO compounds with lone-pair cations.

Acknowledgements

This work is supported by the National Natural Science Foundation of China (Grant Nos. 51962033, 51462033, 11864040), the Natural Science Foundation of Xinjiang Uygur Autonomous Region of China (Grant No. 2017Q013, 2018D01C045, 2018D01C072), the Science and Technology

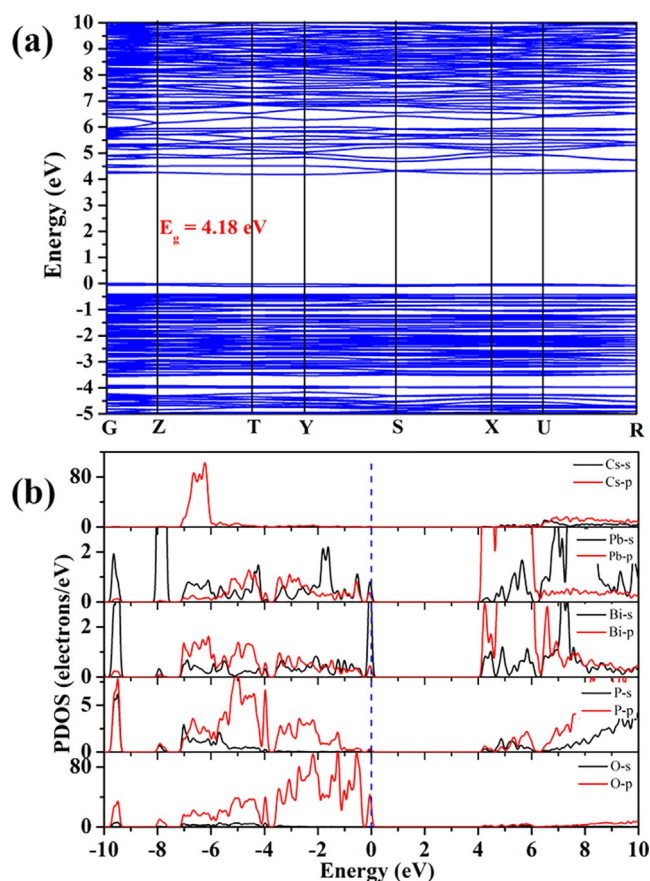


Figure 10. Electronic properties of II. a) Band structure. b) Projected density of states (PDOS).

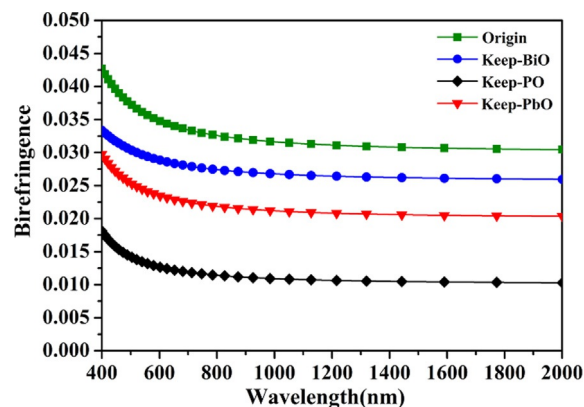


Figure 11. The obtained birefringence of I (RbPbBi531) after the PbO, BiO and PO polyhedra were cut using the real-space atom-cutting method.

Research Program for Colleges and Universities in the Department of Education in Xinjiang Uygur Autonomous Region of China (Grant No. XJEDU2017M006).

Conflict of interest

The authors declare no conflict of interest.

Keywords: [PbPO]_∞ layers · birefringence · phase-matchable · pyrophosphates · SHG responses

- [1] L. Wu, S. Patankar, T. Morimoto, N. L. Nair, E. Thewalt, A. Little, J. G. Analytis, J. E. Moore, J. Orenstein, *Nat. Phys.* **2017**, *13*, 350–355.
- [2] a) Y. X. Song, M. Luo, C. S. Lin, N. Ye, *Chem. Mater.* **2017**, *29*, 896–903; b) E. L. Belokoneva, S. Y. Stefanovich, O. V. Dimitrova, A. S. Karamysheva, A. S. Volkov, *Inorg. Chem.* **2017**, *56*, 1186–1192; c) K. M. Ok, *Acc. Chem. Res.* **2016**, *49*, 2774–2785; d) T. T. Tran, H. Yu, J. M. Rondinelli, K. R. Poeppelmeier, P. S. Halasyamani, *Chem. Mater.* **2016**, *28*, 5238–5258; e) X. X. Jiang, L. Kang, S. X. Luo, P. F. Gong, M. H. Lee, Z. S. Lin, *Int. J. Mod. Phys. B* **2014**, *28*, 1430018.
- [3] a) H. Lee, K. M. Ok, *Bull. Korean Chem. Soc.* **2020**, *41*, 139–142; b) H. Lin, L. Chen, J. S. Yu, H. Chen, L. M. Wu, *Chem. Mater.* **2017**, *29*, 499–503; c) X. H. Dong, L. Huang, C. F. Hu, H. M. Zeng, F. X. Lin, X. Wang, K. M. Ok, G. H. Zou, *Angew. Chem. Int. Ed.* **2019**, *58*, 6528–6534; *Angew. Chem.* **2019**, *131*, 6598–6604.
- [4] a) H. W. Huang, L. J. Liu, S. F. Jin, W. J. Yao, Y. H. Zhang, C. T. Chen, *J. Am. Chem. Soc.* **2013**, *135*, 18319–18322; b) T. T. Tran, N. Z. Koocher, J. M. Rondinelli, P. S. Halasyamani, *Angew. Chem. Int. Ed.* **2017**, *56*, 2969–2973; *Angew. Chem.* **2017**, *129*, 3015–3019; c) G. Zou, C. Lin, H. Jo, G. Nam, T. S. You, K. M. Ok, *Angew. Chem. Int. Ed.* **2016**, *55*, 12078–12082; *Angew. Chem.* **2016**, *128*, 12257–12261.
- [5] C. T. Chen, B. C. Wu, A. D. Jiang, G. M. You, *Sci. China B* **1985**, *28*, 235.
- [6] C. T. Chen, Y. C. Wu, A. D. Jiang, B. C. Wu, G. M. You, R. K. Li, S. J. Lin, *J. Opt. Soc. Am. B* **1989**, *6*, 616–621.
- [7] a) C. T. Chen, G. W. Wang, X. Wang, Z. Y. Xu, *Appl. Phys. B* **2009**, *97*, 9–25; b) C. T. Chen, Z. Y. Xu, D. Q. Deng, J. Zhang, G. K. L. B. Wong, *Appl. Phys. Lett.* **1996**, *68*, 2930–2932.
- [8] G. Q. Zhou, J. Xu, X. D. Chen, H. Y. Zhong, S. T. Wang, K. Xu, P. Z. Deng, F. X. Gan, *J. Cryst. Growth* **1998**, *191*, 517–519.
- [9] X. L. Chen, B. B. Zhang, F. F. Zhang, Y. Wang, M. Zhang, Z. Y. Yang, K. R. Poeppelmeier, S. L. Pan, *J. Am. Chem. Soc.* **2018**, *140*, 16311–16319.
- [10] a) Y. Z. Huang, L. M. Wu, X. T. Wu, L. H. Li, L. Chen, Y. F. Zhang, *J. Am. Chem. Soc.* **2010**, *132*, 12788–12789; b) Y. C. Liu, X. M. Liu, S. Liu, Q. R. Ding, Y. Q. Li, L. Li, S. G. Zhao, Z. S. Lin, J. H. Luo, M. C. Hong, *Angew. Chem. Int. Ed.* **2020**, *59*, 7793–7796; *Angew. Chem.* **2020**, *132*, 7867–7870; c) G. S. Yang, P. F. Gong, Z. S. Lin, N. Ye, *Chem. Mater.* **2016**, *28*, 9122–9131; d) Q. A. Huang, L. J. Liu, X. Y. Wang, R. K. Li, C. T. Chen, *Inorg. Chem.* **2016**, *55*, 12496–12499; e) H. P. Wu, S. L. Pan, K. R. Poeppelmeier, H. Y. Li, D. Z. Jia, Z. H. Chen, X. Y. Fan, Y. Yang, *J. Am. Chem. Soc.* **2011**, *133*, 7786–7790; f) H. P. Wu, H. W. Yu, Z. H. Yang, X. L. Hou, S. L. Pan, X. Su, K. R. Poeppelmeier, J. M. Rondinelli, *J. Am. Chem. Soc.* **2013**, *135*, 4215–4219; g) B. B. Zhang, G. Q. Shi, Z. H. Yang, F. F. Zhang, S. L. Pan, *Angew. Chem. Int. Ed.* **2017**, *56*, 3916–3919; *Angew. Chem.* **2017**, *129*, 3974–3977; h) M. Mutailipu, M. Zhang, B. B. Zhang, L. Y. Wang, Z. Y. Yang, X. Zhou, S. L. Pan, *Angew. Chem. Int. Ed.* **2018**, *57*, 6095–6099; *Angew. Chem.* **2018**, *130*, 6203–6207; i) R. H. Cong, Y. Wang, L. Kang, Z. Y. Zhou, Z. S. Lin, T. Yang, *Inorg. Chem. Front.* **2015**, *2*, 170–176; j) M. Luo, F. Liang, Y. X. Song, D. Zhao, F. Xu, N. Ye, Z. S. Lin, *J. Am. Chem. Soc.* **2018**, *140*, 3884–3887; k) H. K. Liu, Y. Wang, B. B. Zhang, Z. H. Yang, S. L. Pan, *Chem. Sci.* **2020**, *11*, 694–698.
- [11] a) G. Q. Shi, Y. Wang, F. F. Zhang, B. B. Zhang, Z. H. Yang, X. L. Hou, S. L. Pan, K. R. Poeppelmeier, *J. Am. Chem. Soc.* **2017**, *139*, 10645–10648; b) Z. Z. Zhang, Y. Wang, B. B. Zhang, Z. H. Yang, S. L. Pan, *Angew. Chem. Int. Ed.* **2018**, *57*, 6577–6581; *Angew. Chem.* **2018**, *130*, 6687–6691; c) F. Liang, L. Kang, P. F. Gong, Z. S. Lin, Y. C. Wu, *Chem. Mater.* **2017**, *29*, 7098–7102; d) Y. Wang, B. B. Zhang, Z. H. Yang, S. L. Pan, *Angew. Chem. Int. Ed.* **2018**, *57*, 2150–2154; *Angew. Chem.* **2018**, *130*, 2172–2176; e) X. F. Wang, Y. Wang, B. B. Zhang, F. F. Zhang, Z. H. Yang, S. L. Pan, *Angew. Chem. Int. Ed.* **2017**, *56*, 14119–14123; *Angew. Chem.* **2017**, *129*, 14307–14311.
- [12] P. Yu, L. M. Wu, L. J. Zhou, L. Chen, *J. Am. Chem. Soc.* **2014**, *136*, 480–487.
- [13] H. W. Yu, J. Young, H. P. Wu, W. G. Zhang, J. M. Rondinelli, P. S. Halasyamani, *Chem. Mater.* **2017**, *29*, 1845–1855.
- [14] S. G. Zhao, P. F. Gong, S. Y. Luo, L. Bai, Z. S. Lin, Y. Y. Tang, Y. L. Zhou, M. C. Hong, J. H. Luo, *Angew. Chem. Int. Ed.* **2015**, *54*, 4217–4221; *Angew. Chem.* **2015**, *127*, 4291–4295.
- [15] P. Shan, T. Q. Sun, H. Chen, H. D. Liu, S. L. Chen, X. W. Liu, Y. F. Kong, J. J. Xu, *Sci. Rep.* **2016**, *6*, 25201.
- [16] T. Q. Sun, P. Shan, H. Chen, X. W. Liu, H. D. Liu, S. L. Chen, Y. A. Cao, Y. F. Kong, J. J. Xu, *CrystEngComm* **2014**, *16*, 10497–10504.
- [17] J. Chen, L. Xiong, L. Chen, L. M. Wu, *J. Am. Chem. Soc.* **2018**, *140*, 14082–14086.
- [18] a) J. Gopalakrishnan, K. Ramesha, K. K. Rangan, S. Pandey, *J. Solid State Chem.* **1999**, *148*, 75–80; b) G. H. Zou, H. Jo, S. J. Lim, T. S. You, K. M. Ok, *Angew. Chem. Int. Ed.* **2018**, *57*, 8619–8622; *Angew. Chem.* **2018**, *130*, 8755–8758; c) H. G. Kim, T. T. Tran, W. Choi, T. S. You, P. S. Halasyamani, K. M. Ok, *Chem. Mater.* **2016**, *28*, 2424–2432; d) M. K. Kim, S. H. Kim, H. Y. Chang, P. S. Halasyamani, K. M. Ok, *Inorg. Chem.* **2010**, *49*, 7028–7034.
- [19] I. V. Zatovsky, N. Y. Strutynska, Y. A. Hizhnyi, V. N. Baumer, I. V. Ogorodnyk, N. S. Slobodyanik, I. V. Odynets, N. I. Klyui, *Dalton Trans.* **2018**, *47*, 2274–2284.
- [20] M. Wen, H. P. Wu, X. H. Wu, *Inorg. Chem.* **2020**, *59*, 2945–2951.
- [21] P. S. Prangya, T. N. G. Row, *Inorg. Chem.* **2010**, *49*, 10013–10021.
- [22] S. K. Kurtz, T. T. Perry, *J. Appl. Phys.* **1968**, *39*, 3798–3813.
- [23] Y. G. Shen, S. G. Zhao, B. Q. Zhao, C. M. Ji, L. N. Li, Z. H. Sun, M. C. Hong, J. H. Luo, *Inorg. Chem.* **2016**, *55*, 11626–11629.
- [24] S. G. Zhao, Y. Yang, Y. G. Shen, X. D. Wang, Q. G. Ding, X. F. Li, Y. Q. Li, L. N. Li, Z. S. Lin, J. H. Luo, *J. Mater. Chem. C* **2018**, *6*, 3910–3916.
- [25] a) S. G. Zhao, X. Y. Yang, Y. Yang, X. J. Kuang, F. Q. Lu, P. Shan, Z. H. Sun, Z. S. Lin, M. C. Hong, J. H. Luo, *J. Am. Chem. Soc.* **2018**, *140*, 1592–1595; b) X. Y. Yang, S. G. Zhao, S. P. Geng, L. Yang, Q. Z. Huang, X. J. Kuang, J. H. Luo, X. R. Xing, *Chem. Mater.* **2019**, *31*, 9843–9849.
- [26] L. Li, Y. Wang, B. H. Lei, S. J. Han, Z. H. Yang, H. Y. Li, S. L. Pan, *J. Mater. Chem. C* **2017**, *5*, 269–274.
- [27] L. Li, Y. Wang, B. H. Lei, S. J. Han, Z. H. Yang, K. R. Poeppelmeier, S. L. Pan, *J. Am. Chem. Soc.* **2016**, *138*, 9101–9104.
- [28] G. P. Han, Q. Liu, Y. Wang, X. Su, Z. H. Yang, S. L. Pan, *Phys. Chem. Chem. Phys.* **2016**, *18*, 19123–19129.
- [29] H. W. Yu, J. Young, H. P. Wu, W. G. Zhang, J. M. Rondinelli, P. S. Halasyamani, *J. Am. Chem. Soc.* **2016**, *138*, 4984–4989.
- [30] H. W. Yu, W. G. Zhang, J. Young, J. M. Rondinelli, P. S. Halasyamani, *J. Am. Chem. Soc.* **2016**, *138*, 88–91.
- [31] Y. J. Shi, Y. Wang, S. L. Pan, Z. H. Yang, X. Y. Dong, H. P. Wu, M. Zhang, J. Cao, Z. X. Zhou, *J. Solid State Chem.* **2013**, *197*, 128–133.
- [32] S. G. Zhao, P. F. Gong, S. Y. Luo, L. Bai, Z. S. Lin, C. M. Ji, T. L. Chen, M. C. Hong, J. H. Luo, *J. Am. Chem. Soc.* **2014**, *136*, 8560–8563.
- [33] L. Li, S. J. Han, B. H. Lei, Y. Wang, H. Y. Li, Z. H. Yang, S. L. Pan, *Dalton Trans.* **2016**, *45*, 3936–3942.
- [34] P. Shan, T. Q. Sun, H. D. Liu, S. G. Liu, S. L. Chen, X. W. Liu, Y. F. Kong, J. J. Xu, *Cryst. Growth Des.* **2016**, *16*, 5588–5592.
- [35] M. Abudourehman, S. J. Han, B. H. Lei, Z. H. Yang, X. F. Long, S. L. Pan, *J. Mater. Chem. C* **2016**, *4*, 10630–10637.

- [36] F. Kubel, H. Schmid, *Acta Crystallogr. Sect. B* **1990**, *46*, 698–702.
- [37] a) H. Xiao, T. K. Jamil, W. A. Goddard, *J. Phys. Chem. Lett.* **2011**, *2*, 212–217; b) M. K. Chan, G. Ceder, *Phys. Rev. Lett.* **2010**, *105*, 196403.
- [38] a) J. Lin, M. H. Lee, Z. P. Liu, C. Chen, C. Pickard, *Phys. Rev. B* **1999**, *60*, 13380–13389; b) B. B. Zhang, M. H. Lee, Z. H. Yang, Q. Jing, S. L. Pan, M. Zhang, H. P. Wu, X. Su, C. S. Li, *Appl. Phys. Lett.* **2015**, *106*, 031906.
- [39] a) X. Y. Cheng, M. H. Whangbo, G. C. Guo, M. C. Hong, S. Q. Deng, *Angew. Chem. Int. Ed.* **2018**, *57*, 3933–3937; *Angew. Chem.* **2018**, *130*, 3997–4001; b) S. J. Cyvin, J. E. Rauch, J. C. Decius, *J. Chem. Phys.* **1965**, *43*, 4083–4095.

Manuscript received: May 25, 2020
Revised manuscript received: June 14, 2020
Accepted manuscript online: June 19, 2020
Version of record online: August 6, 2020